PHOTONICS Research

Ultralow-quantum-defect Raman laser based on the boson peak in phosphosilicate fiber

Yang Zhang,[1] Jiangming Xu,[1,2] Jun Ye,[1] Jiaxin Song,[1] Tianfu Yao,[1] and Pu Zhou[1,3]

[1]College of Advanced Interdisciplinary Studies, National University of Defense Technology, Changsha 410073, China
[2]e-mail: jmxu1998@163.com
[3]e-mail: zhoupu203@163.com

Received 21 February 2020; revised 17 May 2020; accepted 19 May 2020; posted 19 May 2020 (Doc. ID 390950); published 16 June 2020

Quantum defects (QDs) have always been a key factor of the thermal effect in high-power fiber lasers. Much research on low-QD fiber lasers has been reported in the past decades, but most of it is based on active fibers. Besides, Raman fiber lasers based on the stimulated Raman scattering effect in passive fiber are also becoming an important kind of high-power fiber laser for their unique advantages, such as their significantly broader wavelength-tuning range and being free of photon darkening. In this paper, we demonstrate an ultralow-QD Raman fiber laser based on phosphosilicate fiber. There is a strong boson peak located at a frequency shift of 3.65 THz in the Raman gain spectrum of the phosphosilicate fiber we employed. By utilizing this boson peak to provide Raman gain and adopting an amplified spontaneous emission source at 1066 nm as the pump source, 1080 nm Stokes light is generated, corresponding to a QD of 1.3%. The spectral purity at 1080 nm can be up to 96.03%, and the output power is 12.5 W, corresponding to a conversion efficiency of 67.2%. Moreover, by increasing the pump wavelength to 1072 nm, the QD is reduced to 0.74%, and the output power at 1080 nm is 10.7 W, with a spectral purity of 82.82%. To the best of our knowledge, this is the lowest QD ever reported for Raman fiber lasers. This work proposes a promising way of achieving high-power, high-efficiency Raman fiber lasers.

https://doi.org/10.1364/PRJ.390950

1. INTRODUCTION

Quantum defects (QDs), defined as QD $= 1 - \lambda_p/\lambda_s$ (where λ_p is the pump wavelength and λ_s is the lasing wavelength), have always been a key parameter in high-power fiber lasers. High QD will not only limit the conversion efficiency but also increase the thermal load in fiber lasers. Heavy thermal load may result in some tough issues, such as transverse mode instability and fiber fusing, and thus restrict the power scaling of fiber lasers [1,2]. Hence, much research on low-QD fiber lasers has been reported in the past decades [3–6]. One of the most common ways of reducing QD in fiber lasers is tandem pumping [7–12]. In 2010, researchers from IPG Photonics reported a 10 kW fiber laser pumped at 1018 nm and emitted at 1070 nm, corresponding to a QD of about 4.86% [13]. In 2011, Wirth *et al.* demonstrated a 2.9 kW fiber laser operating at 1071 nm that is tandem-pumped by a 1030 nm thin-disk laser, and the corresponding QD is about 3.83% [14]. To further reduce the QD of fiber lasers, some specially designed active fibers are adopted [15–17]. For example, in 2018, Yu *et al.* demonstrated fiber lasers with less than 1% QD via ytterbium-doped multicomponent fluorosilicate fibers [18]. Above are the reports of low-QD fiber laser based on active fibers. Besides, Raman fiber lasers based on the stimulated Raman scattering (SRS) effect in passive fiber are also becoming an important kind of high-power fiber laser for their unique advantages, such as significantly broader wavelength tuning range and being free of photon darkening [19–22]. Conventional high-power Raman fiber lasers are generally based on pure silica fiber or germanium-doped fiber [23,24], of which the lowest QD ever reported is 1.02%, pumped at 1064 nm and emitted at 1075 nm [25]. However, as the Raman gain in the pure silica fiber or germanium-doped fiber is relatively low at such a small frequency shift, it is difficult to realize high-power efficient Raman output with such low QD, and the reported power of the Stokes light at 1075 nm in Ref. [25] is 1.1 W under a pump power of 6.5 W at 1064 nm.

In contrast, the phosphosilicate-doped passive fiber, different from traditional pure silica fiber or germanium-doped fiber, has a strong boson peak and a Raman gain peak at a frequency shift of ~40 THz in its Raman gain spectrum. The Raman gain peak at the frequency shift of ~40 THz, which is related to the asymmetric stretching vibrations supported by phosphorus-oxygen double bond [26], has been widely adopted in Raman fiber lasers for high-power generation [27], wavelength extending [28–30], and dual-wavelength operation [31]. However, the boson peak in the phosphosilicate fiber, which is typically ascribed to an excess density of vibrational states

[32], has not attracted much attention. From our perspective, owing to the small frequency shift and high gain coefficient, the boson peak in the phosphosilicate fiber could provide a promising solution for low-QD Raman fiber lasers.

Here we demonstrate a Raman fiber laser with an ultralow QD of 1.3% based on phosphosilicate fiber. In the phosphosilicate fiber we employed, there is a strong boson peak located at the frequency shift of 3.65 THz in its Raman gain spectrum. By utilizing this boson peak to provide Raman gain and adopting an amplified spontaneous emission (ASE) source centered at 1066 nm as pump source, Stokes light at 1080 nm is generated, corresponding to a QD of 1.3%. When the pump power reaches 18.6 W, the spectral purity of the 1080 nm Stokes light component reaches a maximum of 96.03%, and the output power is 12.5 W, corresponding to an optical-to-optical conversion efficiency of 67.2%. Moreover, by increasing the pump wavelength to 1072 nm, the QD is reduced to 0.74%, and the output power at 1080 nm is 10.7 W, with a spectral purity of 82.82%. To the best of our knowledge, this is the lowest QD ever reported for Raman fiber lasers.

2. PRINCIPLE AND EXPERIMENTAL SETUP

The Raman gain spectrum of typical phosphosilicate fiber is shown in Fig. 1(a) [27]. Different from conventional silica fiber, except for two Raman gain peaks at frequency shifts of 13.2 THz and 14.7 THz, there are two more Raman gain peaks. One is the phosphorus-related Raman gain peak at a frequency shift of 39.6 THz, and the other one is the boson peak. In the past decades, the boson peak in vitreous glass has been widely studied [33–37]. According to Shuker *et al.*, the intensity of the boson peak in the Raman gain spectrum is proportional to the density of vibrational states $g(w)$ multiplied by the light vibration coupling coefficient (Pockels' coefficient) $C(w)$ [38]. The detailed expression of the intensity of the boson peak as a function of frequency shift w is given by the following equation:

$$I(w) = g(w)C(w)\frac{1 + n(w)}{w}. \tag{1}$$

Here $[1 + n(w)]$ is the Bose–Einstein occupation number for the Stokes component. In 2004, Schroeder *et al.* studied the influence of temperature and pressure on the Raman scattering effect and boson peaks in different glasses [39]. Their results showed that the intensity of the boson peak is closely linked to the temperature, and the frequency shift of the boson peak is related to the pressure effect, while the composition of glass has a great influence on both the intensity and the frequency shift of the boson peak. From the reports above, it can be inferred that the frequency shift and intensity of the boson peak might differ in different fibers (the distribution of the density of vibrational states can be different).

Before the experiment, in order to find the accurate frequency shift of the boson peak, the output of a laser source operating at 1064 nm was injected into the phosphosilicate fiber through a circulator, and the Raman output spectra were monitored by an optical spectrum analyzer with a resolution of 0.02 nm. The Raman output spectra under different pump power levels are shown in Fig. 1(b). As can be expected, except for the two main Raman peaks at frequency shifts of 13.2 THz and 14.7 THz, there is an apparent boson peak in the low-frequency area, located at the frequency shift of 3.65 THz. Besides, due to the relatively low Raman gain, the light component at the frequency shift of 39.6 THz is very weak, and only a small peak can be observed under a maximum pump power of 21.7 W.

The experimental setup of our ultralow-QD Raman fiber laser system is shown in Fig. 2; it consisted of a pump source, a pair of fiber Bragg gratings (FBGs) operating at 1080 nm, and a section of 500 m phosphosilicate fiber. The pump source is a tunable ASE source with a tuning range of 1055–1075 nm [40]. As a comparison, the Raman fiber laser is also pumped by another fiber ring oscillator tunable from 1055 to 1075 nm [41]. Both pump sources are homemade. The output port of the pump source is spliced with a highly reflective FBG operating at 1080 nm, with a reflectivity of 99.2% and 3 dB bandwidth of 1 nm. The core diameter and cladding diameter

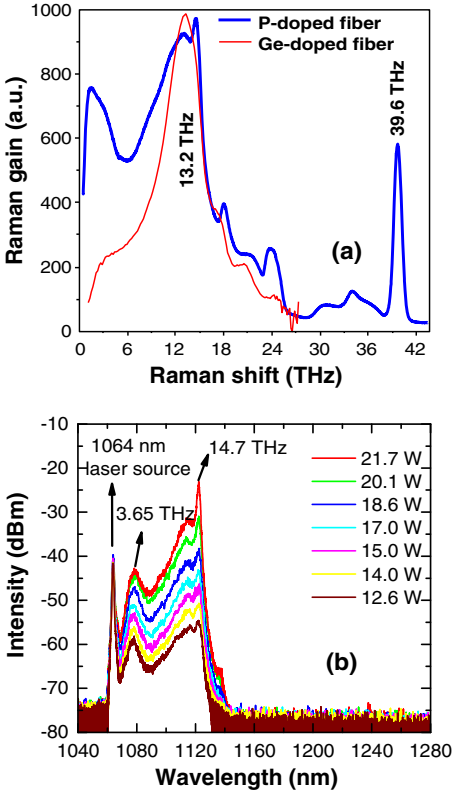

Fig. 1. (a) Typical Raman gain spectrum of phosphosilicate fiber [27]. (b) The Raman output spectra of the phosphosilicate fiber we used under different pump powers.

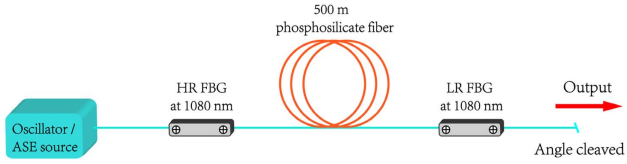

Fig. 2. Experimental setup of our low-quantum-defect Raman fiber laser. ASE, amplified spontaneous emission; HR, highly reflective; FBG, fiber Bragg grating; LR, low reflective.

of the pigtail fiber of the FBG are 10 μm and 125 μm, respectively. After the highly reflective FBG is a section of 500 m phosphosilicate fiber, the core diameter and cladding diameter of which are 5 μm and 125 μm, respectively. The phosphosilicate fiber has a numerical aperture of about 0.18, and the transmission loss at 1080 nm is around 1.56 dB/km. A low reflective FBG operating at 1080 nm with a reflectivity of 10% and 3 dB bandwidth of 0.5 nm is spliced with the output port of the phosphosilicate fiber. The pigtail fiber of the low reflective FBG has the same fiber size as the pigtail fiber of the highly reflective FBG (10/125 μm). An oscillation cavity is established between the highly reflective FBG and the low reflective FBG. Due to the mismatch of the mode field diameter, there is a small splicing loss between the pigtail fiber of the FBG and phosphosilicate fiber, about 0.25 dB after splicing optimization. Moreover, the output port of the Raman fiber laser is 8° cleaved to suppress the Fresnel reflection.

3. RESULT AND DISCUSSION

First, the influence of the pump source on the output characteristics of the 1080 nm Raman fiber laser is studied. The central wavelengths of the oscillator and ASE source are both tuned to 1066 nm, corresponding to the 3.65 THz frequency shift of the boson peak from 1080 nm. The spectral evolution of the 1080 nm Raman fiber laser pumped by the oscillator and the ASE source is shown in Figs. 3(a) and 3(b), respectively. For the oscillator-pumped Raman fiber laser, as the pump power increases, the first-order Stokes light at 1080 nm, corresponding to the boson peak, is generated first. With the further increase of pump power, light components at 1094, 1125, and 1140 nm are generated subsequently. As a result, the spectral purity at 1080 nm is no more than 90%. The generation of the light component at 1094 nm is related to the Raman-assisted three-wave mixing (RATWM) effect [42,43], while light components at 1125 nm and 1140 nm are the result of Raman gain peak at the frequency shift 14.7 THz, pumped by light components at 1066 nm and 1080 nm, respectively. As for the ASE source pumped ones, a similar RATWM phenomenon can be observed, but under the same pump power level, no other light component is observed and the spectral purity is higher. The difference of the output characteristics between the oscillator-pumped Raman fiber laser and ASE-pumped ones is associated with the temporal characteristics of the two pump sources. As has been reported, due to the ultrashort response time of the SRS effect, the Raman conversion process in a Raman fiber laser is closely related to the temporal behavior of the pump source [44–47]. The temporal behaviors of the oscillator and the ASE source are measured with an oscilloscope of 1 GHz bandwidth under the same power level. Figure 3(c) shows the time-domain measurement results in the time scale of 4 μs. It is apparent that the output of the oscillator has bigger temporal fluctuation than the ASE source, with a peak-to-peak fluctuation of 102% and standard deviation of 12.6%. In stark contrast, the peak-to-peak fluctuation of the ASE source is 18%, and the standard deviation is 1.9%. Under the same average power, a pump source with bigger temporal fluctuation has higher peak power compared to a temporally stable laser source, as a result of which, spontaneous Stokes components at the

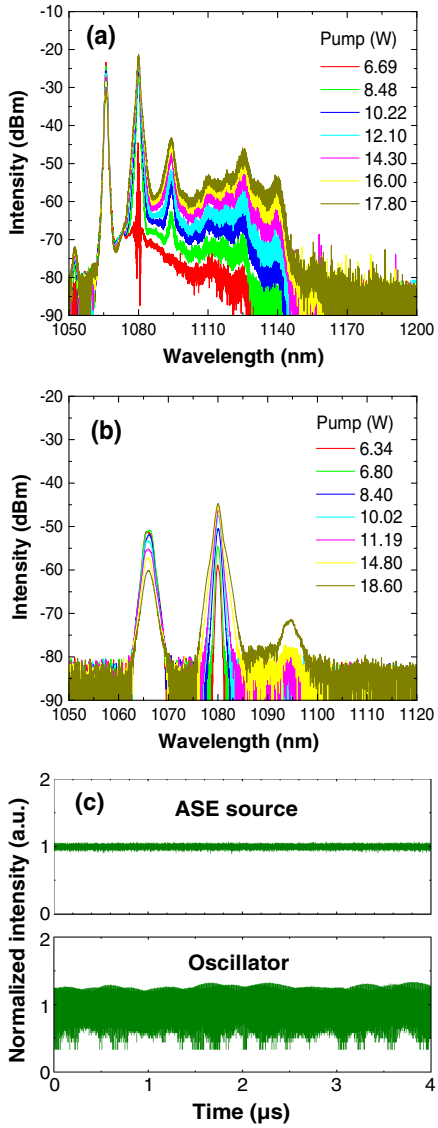

Fig. 3. (a) Spectral evolution of the oscillator-pumped Raman fiber laser. (b) Spectral evolution of the ASE-source-pumped Raman fiber laser. (c) Temporal behaviors of the oscillator and ASE source under the same power level.

frequency shift of 14.7 THz can be generated more easily and the spectral purity at 1080 nm is decreased.

Figure 4(a) shows the total output, Raman output, and residual pump power of the ASE-source-pumped Raman fiber laser as a function of the pump power. When the pump power exceeds 6 W, Stokes light at 1080 nm is generated. When the pump power reaches 18.6 W, the output power at 1080 nm is 12.5 W, and the corresponding output spectrum is shown in Fig. 4(b). The intensity of the 1080 nm Stokes light component is 15.4 dB higher than the residual pump and 26.7 dB higher than the RATWM-related light component at around 1094 nm, and the spectral purity of the 1080 nm Stokes light component reaches a maximum of 96.03%. The inset figure shows the corresponding output spectrum in linear scale. Moreover, the optical-to-optical conversion efficiency is 67.2%,

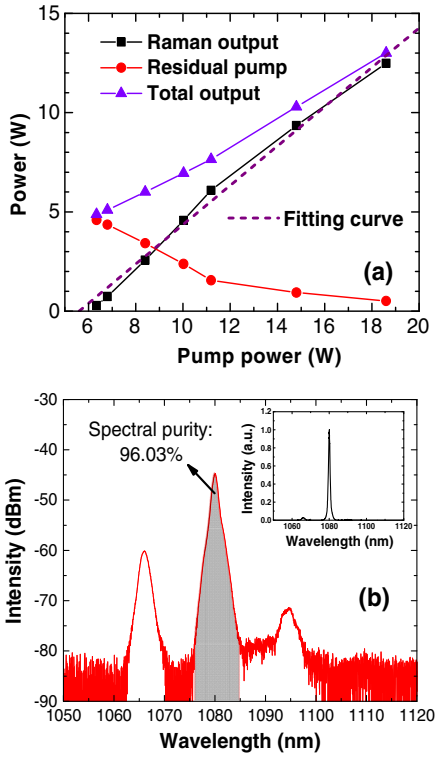

Fig. 4. (a) Total output, Raman output, and residual pump power of the ASE-source-pumped Raman fiber laser as a function of pump power. (b) Output spectrum of the ASE-pumped Raman fiber laser with a spectral purity of 96.03% (inset: the corresponding output spectrum in linear scale).

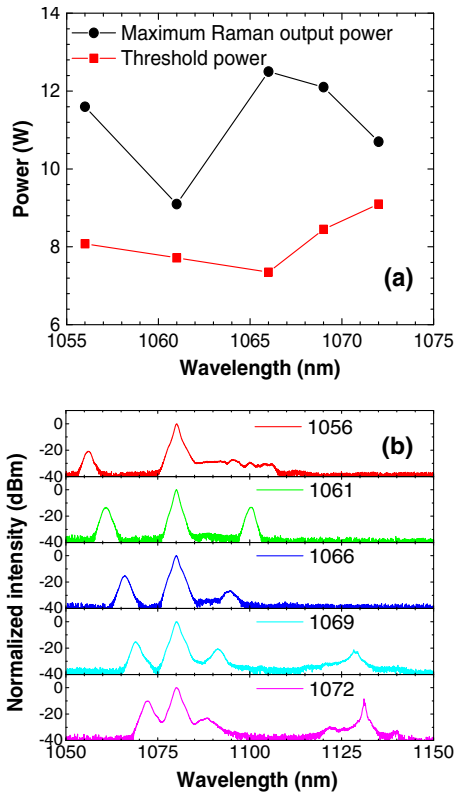

Fig. 5. (a) Threshold power, maximum Raman output power, and (b) corresponding output spectra at the same pump level of the ASE-source-pumped Raman fiber laser under different pump wavelengths.

and the slope efficiency is up to 99.2% (higher than the quantum efficiency). The slope efficiency is defined as slope of the curve obtained by plotting the output power versus the pump power. As the SRS is a nonlinear process, when the pump power is above the threshold, the residual pump will be converted into the Stokes light more completely with the further increase of the pump power, and thus the slope efficiency may exceed the quantum efficiency. Considering a transmission loss of 25% of this phosphosilicate fiber, the efficiency of our Raman fiber laser is impressive. The further increase of output power is limited by the RATWM effect, as the RATWM-effect-generated 1094 nm light component may be injected into the employed pump source and threaten the operating safety. Compared to previously reported low-QD fiber laser based on ytterbium-doped multicomponent fluorosilicate optical fiber [18], which has a maximum output power of ~0.4 W and a maximum slope efficiency of 62.1% (limited by ASE and background loss), our result shows significant improvement in output power, and the efficiency is higher.

Next, we studied the influence of the ASE pump source's wavelength on the Raman fiber laser's output characteristics. Five different wavelengths (1056, 1061, 1066, 1069, and 1072 nm) are adopted, while the 3 dB linewidth of the ASE pump source is fixed at 2 nm. Figure 5(a) shows the threshold power and maximum Raman output power of the 1080 nm Raman fiber laser under different pump wavelengths. It can be seen that when the pump wavelength is 1066 nm, corresponding to a QD of 1.3%, the threshold power is the lowest while the Raman output power is the highest; they are 7.35 W and 12.5 W, respectively. The frequency shift between 1066 nm and 1080 nm is 3.65 THz, corresponding to the boson peak of the phosphosilicate fiber we used, and thus the Raman gain at 1080 nm is the highest under this pump wavelength. Consequently, the threshold power is the lowest and the output power is the highest. Figure 5(b) shows the output spectra for different pump wavelengths under the same pump power of 18.6 W. An obvious three-wave mixing effect can be observed under pump wavelengths of 1061, 1066, 1069, and 1072 nm. Among these four, the RATWM-related peak under a pump wavelength of 1066 nm is the weakest. As we have not concluded a perfect explanation for this phenomenon presently, we will carry out further research to have a deeper understanding of the three-wave mixing effect in Raman fiber lasers. Moreover, when the pump wavelength is 1069 nm or 1072 nm, the Raman gain is not high enough to suppress the Raman gain at the frequency shift of 14.7 THz, and an unwanted spontaneous Stokes light component is generated with the further increasing of the pump power; thus, the output power and spectral purity at 1080 nm are limited. When the pump wavelength is 1072 nm, the lowest QD of 0.74% is realized. The corresponding maximum output power at 1080 nm is 10.7 W with a spectral purity of 82.82%.

4. CONCLUSION

In conclusion, we demonstrate a Raman fiber laser with an ultralow QD of 1.3% based on a section of 500 m phosphosilicate fiber. There is a strong boson peak at frequency shift of 3.65 THz in the Raman gain spectrum of the phosphosilicate fiber we employed. By utilizing this boson peak to provide Raman gain and adopting a temporally stable ASE source operating at 1066 nm as the pump source, Stokes light at 1080 nm is generated. When the pump power reaches 18.6 W, the spectral purity of the 1080 nm Stokes light component can be up to 96.03% with an output power of 12.5 W. The corresponding optical-to-optical conversion efficiency is 67.2%. Moreover, by increasing the pump wavelength to 1072 nm, the QD is reduced to 0.74%, and the output power at 1080 nm is 10.7 W with a spectral purity of 82.82%. The further power scaling is restricted by the spontaneous Stokes light emission at the frequency shift of 14.7 THz. Owing to the ultralow QD, the Raman fiber laser we proposed shows great potential in achieving high-power, high-efficiency laser output. In future work, we will optimize the operating parameters for higher output power.

Funding. National Natural Science Foundation of China (NSFC) (61635005, 61905284); National Postdoctoral Program for Innovative Talents (BX20190063); Hunan Innovative Province Construction Project (2019RS3017); Huo Yingdong Education Foundation (151062).

Acknowledgment. We are grateful to Sen Guo for his help with this work.

Disclosures. The authors declare that there are no conflicts of interest related to this paper.

REFERENCES

1. R. Kashyap and K. J. Blow, "Observation of catastrophic self-propelled self-focusing in optical fibres," Electron. Lett. **24**, 47–49 (1988).
2. C. Jauregui, J. Limpert, and A. Tunnermann, "High-power fibre lasers," Nat. Photonics **7**, 861–867 (2013).
3. S. Matsubara, K. Uno, Y. Nakajima, S. Kawato, T. Kobayashi, and A. Shirakawa, "Extremely low quantum defect oscillation of ytterbium fiber laser by laser diode pumping at room temperature," in *Advanced Solid-State Photonics*, OSA Technical Digest Series (Optical Society of America, 2007), paper TuB4.
4. T. Yao, J. Ji, and J. Nilsson, "Ultra-low quantum-defect heating in ytterbium-doped aluminosilicate fibers," J. Lightwave Technol. **32**, 429–434 (2014).
5. M. Dubinskii, J. Zhang, and V. Ter-Mikirtychev, "Highly scalable, resonantly cladding-pumped, Er-doped fiber laser with record efficiency," Opt. Lett. **34**, 1507–1509 (2009).
6. S. R. Bowman, "Low quantum defect laser performance," Opt. Eng. **56**, 011104 (2016).
7. C. A. Codemard, J. K. Sahu, and J. Nilsson, "Tandem cladding-pumping for control of excess gain in ytterbium-doped fiber amplifiers," IEEE J. Quantum Electron. **46**, 1860–1869 (2010).
8. M. A. Jebali, J.-N. Maran, and S. LaRochelle, "264 W output power at 1585 nm in Er-Yb codoped fiber laser using in-band pumping," Opt. Lett. **39**, 3974–3977 (2014).
9. Y. Wang, J. Yang, C. Huang, Y. Luo, S. Wang, Y. Tang, and J. Xu, "High power tandem-pumped thulium-doped fiber laser," Opt. Express **23**, 2991–2998 (2015).
10. H. Xiao, J. Leng, H. Zhang, L. Huang, J. Xu, and P. Zhou, "High-power 1018 nm ytterbium-doped fiber laser and its application in tandem pump," Appl. Opt. **54**, 8166–8169 (2015).
11. P. Ma, H. Xiao, D. Meng, W. Liu, R. Tao, J. Leng, Y. Ma, R. Su, P. Zhou, and Z. Liu, "High power all-fiberized and narrow-bandwidth MOPA system by tandem pumping strategy for thermally induced mode instability suppression," High Power Laser Sci. Eng. **6**, e57 (2018).
12. Z. Wang, P. Yan, Y. Huang, J. Tian, C. Cai, D. Li, Y. Yi, Q. Xiao, and M. Gong, "An efficient 4-kW level random fiber laser based on a tandem-pumping scheme," IEEE Photon. Technol. Lett. **31**, 817–820 (2019).
13. E. Stiles, "New developments in IPG fiber laser technology," in *Proceedings of the 5th International Workshop on Fiber Lasers* (2009).
14. C. Wirth, O. Schmidt, A. Kliner, T. Schreiber, R. Eberhardt, and A. Tunnermann, "High-power tandem pumped fiber amplifier with an output power of 2.9 kW," Opt. Lett. **36**, 3061–3063 (2011).
15. G. Gu, Z. Liu, F. Kong, H. Tam, R. K. Shori, and L. Dong, "Highly efficient ytterbium-doped phosphosilicate fiber lasers operating below 1020 nm," Opt. Express **23**, 17693–17700 (2015).
16. S. Suzuki, H. A. McKay, X. Peng, L. Fu, and L. Dong, "Highly ytterbium-doped silica fibers with low photo-darkening," Opt. Express **17**, 9924–9932 (2009).
17. M. Cavillon, C. Kucera, T. W. Hawkins, N. Yu, P. Dragic, and J. Ballato, "Ytterbium-doped multicomponent fluorosilicate optical fibers with intrinsically low optical nonlinearities," Opt. Mater. Express **8**, 744–760 (2018).
18. N. Yu, M. Cavillon, C. Kucera, T. W. Hawkins, J. Ballato, and P. Dragic, "Less than 1% quantum defect fiber lasers via ytterbium-doped multicomponent fluorosilicate optical fiber," Opt. Lett. **43**, 3096–3099 (2018).
19. Y. Feng, *Raman Fiber Lasers* (Springer, 2017).
20. D. Georgiev, V. P. Gapontsev, A. G. Dronov, M. Y. Vyatkin, A. B. Rulkov, S. V. Popov, and J. R. Taylor, "Watts-level frequency doubling of a narrow line linearly polarized Raman fiber laser to 589 nm," Opt. Express **13**, 6772–6776 (2005).
21. L. Zhang, H. Jiang, X. Yang, W. Pan, S. Cui, and Y. Feng, "Nearly-octave wavelength tuning of a continuous wave fiber laser," Sci. Rep. **7**, 42611 (2017).
22. R. Cao, G. Chen, Y. Chen, Z. Zhang, X. Lin, B. Dai, L. Yang, and J. Li, "Effective suppression of the photodarkening effect in high-power Yb-doped fiber amplifiers by H_2 loading," Photon. Res. **8**, 288–295 (2020).
23. V. R. Supradeepa and J. W. Nicholson, "Power scaling of high-efficiency 1.5 μm cascaded Raman fiber lasers," Opt. Lett. **38**, 2538–2541 (2013).
24. Y. Chen, T. Yao, L. Huang, H. Xiao, J. Leng, and P. Zhou, "2 kW high-efficiency Raman fiber amplifier based on passive fiber with dynamic analysis on beam cleanup and fluctuation," Opt. Express **28**, 3495–3504 (2020).
25. E. Belanger, M. Bernier, D. Faucher, D. Cote, and R. Vallee, "High-power and widely tunable all-fiber Raman laser," J. Lightwave Technol. **26**, 1696–1701 (2008).
26. E. M. Dianov and A. M. Prokhorov, "Medium-power CW Raman fiber lasers," IEEE J. Sel. Top. Quantum Electron. **6**, 1022–1028 (2000).
27. J. Dong, L. Zhang, J. Zhou, W. Pan, X. Gu, and Y. Feng, "More than 200 W random Raman fiber laser with ultra-short cavity length based on phosphosilicate fiber," Opt. Lett. **44**, 1801–1804 (2019).
28. N. S. Kim, M. Prabhu, C. Li, J. Song, and K. Ueda, "1239/1484 nm cascaded phosphosilicate Raman fiber laser with CW output power of 1.36 W at 1484 nm pumped by CW Yb-doped double-clad fiber laser at 1064 nm and spectral," Opt. Commun. **176**, 219–222 (2000).
29. S. A. Babin, I. D. Vatnik, A. Y. Laptev, M. M. Bubnov, and E. M. Dianov, "High-efficiency cascaded Raman fiber laser with random distributed feedback," Opt. Express **22**, 24929–24934 (2014).
30. I. A. Lobach, S. I. Kablukov, and S. A. Babin, "Linearly polarized cascaded Raman fiber laser with random distributed feedback operating beyond 1.5 μm," Opt. Lett. **42**, 3526–3529 (2017).
31. J. Song, J. Xu, Y. Zhang, J. Ye, and P. Zhou, "Phosphosilicate fiber-based dual-wavelength random fiber laser with flexible power proportion and high spectral purity," Opt. Express **27**, 23095–23102 (2019).

32. H. Tanaka and H. Shintani, "Universal link between the boson peak and transverse phonons in glass," Nat. Mater. **7**, 870–877 (2008).
33. S. N. Taraskin and S. R. Elliott, "Nature of vibrational excitations in vitreous silica," Phys. Rev. B **56**, 8605–8622 (1997).
34. S. N. Taraskin, Y. L. Loh, G. Natarajan, and S. R. Elliott, "Origin of the Boson peak in systems with lattice disorder," Phys. Rev. Lett. **86**, 1255–1258 (2001).
35. V. L. Gurevich, D. A. Parshin, and H. R. Schober, "Anharmonicity, vibrational instability, and the Boson peak in glasses," Phys. Rev. B **67**, 094203 (2003).
36. D. A. Parshin, H. R. Schober, and V. L. Gurevich, "Vibrational instability, two-level systems, and the boson peak in glasses," Phys. Rev. B **76**, 064206 (2007).
37. A. Marruzzo, W. Schirmacher, A. Fratalocchi, and G. Ruocco, "Heterogeneous shear elasticity of glasses: the origin of the boson peak," Sci. Rep. **3**, 1407 (2013).
38. R. Shuker and R. W. Gammon, "Raman-scattering selection-rule breaking and the density of states in amorphous materials," Phys. Rev. Lett. **25**, 222–225 (1970).
39. J. Schroeder, W. Wu, J. L. Apkarian, M. Lee, L. Hwa, and C. T. Moynihan, "Raman scattering and boson peaks in glasses: temperature and pressure effects," J. Non-Cryst. Solids **349**, 88–97 (2004).
40. J. Ye, J. Xu, Y. Zhang, J. Song, J. Leng, and P. Zhou, "Spectrum-manipulable hundred-watt-level high power superfluorescent fiber source," J. Lightwave Technol. **37**, 3113–3118 (2019).
41. J. Song, H. Wu, J. Ye, H. Zhang, J. Xu, P. Zhou, and Z. Liu, "Investigation on extreme frequency shift in silica fiber-based high-power Raman fiber laser," High Power Laser Sci. Eng. **6**, e28 (2018).
42. T. Sylvestre, H. Maillotte, E. Lantz, and P. Tchofo Dinda, "Raman-assisted parametric frequency conversion in a normally dispersive single-mode fiber," Opt. Lett. **24**, 1561–1563 (1999).
43. P. Tchofo, E. Sève, G. Millot, T. Sylvestre, H. Maillote, and E. Lantz, "Raman-assisted three-wave mixing of non-phase-matched waves in optical fibres: application to wide-range frequency conversion," Opt. Commun. **192**, 107–121 (2001).
44. G. P. Agrawal, *Nonlinear Fiber Optics*, 5th ed. (Academic, 2013).
45. J. Dong, L. Zhang, H. Jiang, X. Yang, W. Pan, S. Cui, X. Gu, and Y. Feng, "High order cascaded Raman random fiber laser with high spectral purity," Opt. Express **26**, 5275–5280 (2018).
46. Y. Zhang, J. Song, J. Ye, J. Xu, T. Yao, and P. Zhou, "Tunable random Raman fiber laser at 1.7 μm region with high spectral purity," Opt. Express **27**, 28800–28807 (2019).
47. V. Balaswamy, S. Ramachandran, and V. R. Supradeepa, "High-power, cascaded random Raman fiber laser with near complete conversion over wide wavelength and power tuning," Opt. Express **27**, 9725–9732 (2019).